Time-dependent approach to electron scattering and ionization in the s-wave model

W. Ihra,* M. Draeger, G. Handke,† and H. Friedrich
Physik Department, Technische Universität München, 85747 Garching, Germany
(Received 10 April 1995)

The time-dependent Schrödinger equation is integrated for continuum states of two-electron atoms in the framework of the s-wave model, in which both electrons are restricted to having vanishing individual orbital angular momenta. The method is suitable for studying the time evolution of correlations in the two-electron wave functions and yields probabilities for elastic and inelastic electron scattering and for electron-impact ionization. The spin-averaged probabilities for electron-impact ionization of hydrogen in the s-wave model reproduce the shape of the experimentally observed integrated ionization cross section remarkably well for energies near and above the maximum.

PACS number(s): 34.80.Dp

I. INTRODUCTION

The correlated motion of two electrons in the Coulomb field of an atomic nucleus constitutes one of the most interesting and fundamental problems of atomic physics. There has been considerable progress in the last few years, e.g., in measuring doubly excited states of the helium atom with both principal quantum numbers near or above 7 [1–3], and in reproducing the experimental cross section for electron-impact ionization of hydrogen on the basis of an *ab initio* calculation [4]. Many aspects of two-electron atoms are, however, still far from being fully understood, e.g., the role of the largely (but not completely) chaotic classical dynamics of the three-body Coulomb problem [5] and the asymptotic structure of the wave function describing two electrons in the continuum [6].

Considerable attention has recently been given to one-dimensional models of two-electron atoms, defined by two spatial coordinates, r_1 and r_2, corresponding to the distances of the two electrons from the nucleus [7–16]. A semiclassical understanding of bound and resonant states of real helium has been achieved by Richter and Wintgen on the basis of the collinear model, in which both electrons are restricted to be on opposite sides of the nucleus, corresponding to maximal angular correlations between the two electrons [7,8]. A further approximation to the collinear model has been studied by Grobe and co-workers [10,11], who regularized the singularities of Coulomb potentials at the origin. The present authors have studied in some detail the s-wave model, which is complementary to the collinear model in that both electrons are restricted to spherical states and all angular correlations are eliminated [9,12–14]. The classical dynamics of this model are described in [9,12,13]. Below the breakup threshold the classical dynamics of the s-wave model are remarkably similar to the classical dynamics of the collinear model, in which angular correlations between the two electrons are maximal [9]. A comprehensive account of the quantum-mechanical bound and resonant states of s-wave helium ($Z=2$) for energies below the breakup threshold is given in [14]. The bound $1sns$ states of real helium are described well in this model. The s-wave model is not so realistic near the breakup threshold, where angular correlations are important and the collinear model is more appropriate [15,16]. The threshold region in the s-wave model is of some theoretical interest, because the ionization process is classically forbidden for a finite range of positive energies [12], and the relation between the quantum-mechanical evolution and the classical dynamics is not yet understood in this region.

This paper is devoted to a quantum-mechanical study of continuum states in the s-wave model, and the method we use is the direct integration of the time-dependent Schrödinger equation. This makes it possible to study electron-impact ionization involving two escaping continuum electrons, without having to specify the boundary conditions of the wave function in coordinate space. We give a brief outline of the s-wave model in Sec. II. In Sec. III we describe the time-dependent integration method and illustrate its usefulness for studying the decay of autoionizing states and the evolution of two-particle correlations in the two-electron wave function. In Sec. IV we present probabilities for elastic and inelastic electron scattering by hydrogen as well as for ionization, and we compare them with results from related work. The spin-averaged probabilities for electron-impact ionization of hydrogen reproduce the shape of the experimentally observed cross section [17] remarkably well, better in fact than all previous calculations, except for the essentially exact *ab initio* calculation of Bray and Stelbovics [4].

II. S-WAVE MODEL FOR TWO-ELECTRON ATOMS

Assuming infinite nuclear mass, the Hamiltonian of a two-electron atom is (in atomic units)

$$H=-\frac{1}{2}\vec{\nabla}_1^2-\frac{1}{2}\vec{\nabla}_2^2-\frac{Z}{r_1}-\frac{Z}{r_2}+\frac{1}{|\vec{r}_1-\vec{r}_2|}. \tag{1}$$

In the subspace defined by individual angular momentum zero of both electrons, the interaction potential

*Present address: Department of Mathematics, Royal Holloway and Bedford New College, Egham, Surrey TW20 0EX, England.
†Present address: Dipartimento di Chimica, via Elce di Sotto 8, Perugia, Italy.

$$\frac{1}{|\vec{r}_1-\vec{r}_2|}=\sum_{l=0}^{\infty}\frac{r_<^l}{r_>^{l+1}}P_l(\cos\theta) \tag{2}$$

contributes only the first term in the sum, and the Hamiltonian of the s-wave model is

$$H_s=-\frac{1}{2}\frac{\partial^2}{\partial r_1^2}-\frac{1}{2}\frac{\partial^2}{\partial r_2^2}+V(r_1,r_2), \tag{3}$$

with the total potential

$$V(r_1,r_2)=-\frac{Z}{r_1}-\frac{Z}{r_2}+\frac{1}{r_>}. \tag{4}$$

$r_>$ denotes the larger of the two radii r_1 and r_2. As long as $r_1>r_2$ or $r_1<r_2$ the electrons move independently, the inner electron is affected by the naked nuclear charge Z and the outer electron is affected by a screened charge $Z-1$. The Schrödinger equation of the s-wave model is separable in these regions, but coupling is introduced by the requirement of continuous matching at the boundary $r_1=r_2$.

The s-wave model is a one-dimensional model with two degrees of freedom, viz., the radial coordinates r_1 and r_2 of the two electrons. The assumption of spherical states eliminates all angular correlations between the two electrons. The s-wave model is thus complementary to the collinear model [8], in which both electrons are on opposite sides of the nucleus with maximal angular correlations, and where the interaction potential of the two electrons is $1/(r_1+r_2)$, instead of $1/r_>$ as in (4). The regularized modification of the collinear model as studied by Grobe and co-workers [10,11] is obtained replacing $1/r$ by $1/\sqrt{1+r^2}$ in the various potential terms.

Relativistic effects are not included in (3), but we distinguish singlet ($S=0$) and triplet ($S=1$) coupling of the two-electron spins by requiring the spatial wave function $\Psi(r_1,r_2;t)$ to be symmetric or antisymmetric, respectively,

$$\Psi^{(S=0)}(r_1,r_2;t)=\frac{1}{\sqrt{2}}[\Psi(r_1,r_2;t)+\Psi(r_2,r_1;t)], \tag{5}$$

$$\Psi^{(S=1)}(r_1,r_2;t)=\frac{1}{\sqrt{2}}[\Psi(r_1,r_2;t)-\Psi(r_2,r_1;t)]. \tag{6}$$

Unless explicitly stated otherwise, we shall always assume that the wave functions are symmetrized or antisymmetrized as in (5), (6), and equations which do not refer to $S=0$ or $S=1$ apply to both cases.

In a typical scattering situation one electron approaches with an impact energy $E_{\rm in}=k^2/2$ while the other electron is initially in a bound state of the nuclear Coulomb potential, characterized by its principal quantum number n_i (which we assume to be one). We are studying electron scattering by hydrogen, so $Z=1$. The probabilities for scattering to a final state, in which one electron is in the bound state with quantum number n, are described by the S-matrix element $S_{1,n}$. Since the whole model is one dimensional, the usual cross sections for elastic and inelastic scattering are replaced by dimensionless probabilities, which are related to the S matrix by

$$P_n=|S_{1,n}|^2. \tag{7}$$

The probability for ionizing to a final state with both electrons in the continuum (integrated over the distribution of the available energy among the two electrons) is also a dimensionless quantity, $P_{(e,2e)}$, and the conservation of probability requires

$$\sum_{n=1}^{\infty}|S_{1,n}|^2+P_{(e,2e)}=1. \tag{8}$$

The potential (4) has been used by several authors as a model potential in the Hamiltonian for two electrons in three-dimensional space [18–22]. The Hamiltonian with this potential conserves not only total (orbital) angular momentum, but also the individual angular momenta of both electrons. If we assume an initial state with one electron bound in the $1s$ hydrogen ground state and total orbital angular momentum zero, then all orbital angular momenta are zero and remain zero. In the three-dimensional picture, the same S-matrix elements as occur in Eqs. (7), (8) define the elastic, inelastic, and ionization cross sections which are isotropic and have the dimensions of areas. The S-matrix elements are related to the (angle-independent) scattering amplitudes $f_{1,n}$ by

$$2i\sqrt{kk_n}f_{1,n}=S_{1,n}-\delta_{1,n}. \tag{9}$$

The integrated elastic ($n=1$) and inelastic ($n>1$) scattering cross sections are then given by

$$\sigma_n=4\pi\frac{k_n}{k}|f_{1,n}|^2=\frac{\pi}{k^2}|S_{1,n}-\delta_{1,n}|^2, \tag{10}$$

and the conservation of particle number is expressed via the optical theorem,

$$\mathrm{Im}(f_{1,1})=\frac{1}{2k}\mathrm{Re}(1-S_{1,1})=\frac{k}{4\pi}\left(\sum_{n=1}^{\infty}\sigma_n+\sigma_{(e,2e)}\right), \tag{11}$$

where $\sigma_{(e,2e)}$ is the cross section for ionization, integrated over the distribution of available energy among the two escaping electrons. With (10) Eq. (11) reduces to

$$\sum_{n=1}^{\infty}|S_{1,n}|^2+\frac{k^2}{\pi}\sigma_{(e,2e)}=1, \tag{12}$$

which agrees with (8) when we equate

$$\sigma_{(e,2e)}=\frac{\pi}{k^2}P_{(e,2e)}. \tag{13}$$

Except for the elastic scattering cross section, the cross sections of the three-dimensional model based on the potential (4) (and total angular momentum zero) are merely the dimensionless probabilities of the one-dimensional s-wave model multiplied by the area π/k^2, which is inversely proportional to the impact energy of the incoming projectile electron. This simply expresses the decrease of the weight of the component with total angular momentum zero in the incoming wave as the projectile energy increases. The elastic

scattering cross section in the three-dimensional picture also contains the interference of the scattered wave and the incoming wave, an effect which is absent in the one-dimensional model.

III. SOLVING THE TIME-DEPENDENT SCHRÖDINGER EQUATION

The difficulties associated with formulating the correct asymptotic boundary conditions [6] for the eigenstates of the three-particle Coulomb Hamiltonian (3) can be circumvented by solving the time-dependent Schrödinger equation

$$i\frac{\partial}{\partial t}\Psi(r_1,r_2;t)=H_s\Psi(r_1,r_2;t), \tag{14}$$

starting from an initial wave function at time $t=0$. The wave function must vanish along the coordinate axes,

$$\Psi(r_1=0,r_2;t)=\Psi(r_1,r_2=0;t)=0 \quad \text{at all times } t. \tag{15}$$

On the diagonal $r_1=r_2$ the antisymmetric wave functions vanish and the symmetric wave functions have vanishing derivative perpendicular to the diagonal. We found it practicable to propagate the unsymmetrized wave function and extract the singlet and triplet components by symmetrizing or antisymmetrizing *a posteriori*; this is permissible, because the Schrödinger equation (14) conserves exchange symmetry.

In order to time iterate the wave function we use an implicit operator splitting scheme combined with finite element representations (FER) of the operators in coordinate space, as first introduced by Bottcher [23]. Introducing the split Hamiltonians

$$H_j=-\frac{1}{2}\frac{\partial^2}{\partial r_j^2}+\frac{1}{2}V(r_1,r_2) \quad (j=1,2), \tag{16}$$

the implicit equation

$$\left(1+\frac{i}{2}H_2\Delta t\right)\left(1+\frac{i}{2}H_1\Delta t\right)\Psi(t+\Delta t) =\left(1-\frac{i}{2}H_2\Delta t\right)\left(1-\frac{i}{2}H_1\Delta t\right)\Psi(t) \tag{17}$$

has to be solved in coordinate space. The split-operator method corresponds to propagation of the wave function along one of the coordinates over one half time step Δt, while the second coordinate is kept constant. In the second half of each time step the roles of the coordinates are interchanged. Instead of discretizing the operators on a one-dimensional equally spaced lattice we expand the wave function in linear B splines, thus taking the singularity of the potential at $r_j=0$ properly into account. A detailed description of the method is given in [23–25].

Grobe and co-workers solved the time-dependent Schrödinger equation for their one-dimensional model of two-electron atoms using the method of fast Fourier transforms (FFT) and an equally spaced discrete grid supporting the wave functions [10,11]. However, their model works with regularized Coulomb interactions, and we believe that the FER method is superior for potentials with singularities. The time required by the FER method compares well with that of the FFT method, which scales as $N^2/\ln N$ per time step, where N is the number of lattice points along one axis [26]. In the FER method the operators reduce to tridiagonal matrices. The solution of a linear equation involving a tridiagonal matrix scales as N, and N such calculations with one of the coordinates fixed have to be performed during one time step, thus making the total effort per time step proportional to N^2.

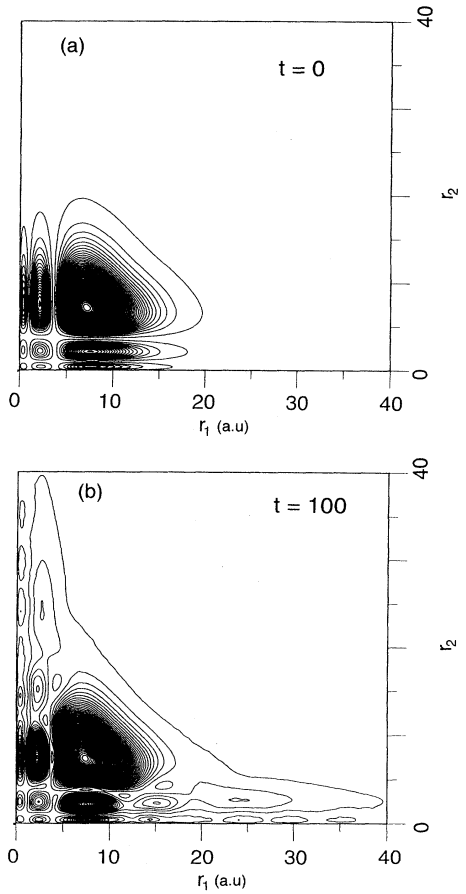

FIG. 1. Contour plot of the density $|\Psi(r_1,r_2)|^2$ of the initially bound (closed-channel) part of the wave function for the $3s3s$ singlet state of s-wave helium ($Z=2$) [14] at time $t=0$ (a) and of the state into which the wave function has evolved after $t=100$ a.u. (b).

One test of the efficacy of this time-dependent method is to calculate the decay of an autoionizing doubly excited state. Energies and widths of doubly excited states of s-wave helium ($Z=2$) have recently been calculated by Draeger *et al.* [14] by solving the time-independent Schrödinger equation. Near the energy of an autoionizing resonance the wave function contains localized (closed-channel) and scattering (open-channel) components, and the resonance widths can, e.g., be derived from the asymptotic phase shifts of the scattering components or, as long as they are sufficiently small, perturbatively using the golden rule. Figure 1(a) shows a density plot of the closed-channel part of the $3s3s$-($^1S_0$) resonance of s-wave helium from Ref. [14]. The

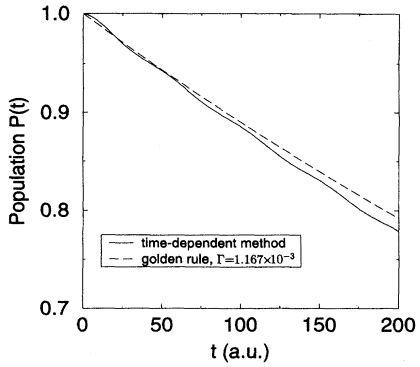

FIG. 2. The solid line shows the time dependence of the population (18) of the $3s3s$ state of s-wave helium ($Z=2$). The dashed line shows the exponential decay $P=\exp(-\Gamma t)$ with the width $\Gamma=0.001\ 167$ a.u. as derived via the golden rule in [14].

$N=n=3$ double excitation is well recognizable by its nodal pattern in the one-particle coordinates r_1 and r_2.

The time evolution of the autoionizing resonance was studied by iterating according to the procedure described above, starting from the closed-channel component of the resonant wave function as initial state $\Psi_i(r_1,r_2)=\Psi(r_1,r_2;t=0)$. The two-electron wave function was iterated on a grid with spacing 0.1 a.u. for $0\leq r_j\leq 5.0$ a.u., spacing 0.2 a.u. for $5.0\leq r_j\leq 15.0$ a.u., and a spacing of 0.5 a.u. for $r_j>15.0$ a.u. ($j=1,2$). We chose the time step to be $\Delta t=0.1$. Figure 1(b) shows the state into which the initial wave function of Fig. 1(a) has evolved after a time span of $t=100$ a.u. Part of the wave function has spread out along the axes as one electron is ionized while the other electron is left behind in the $N=1$ or 2 bound state of the He^+ ion.

The decay of the population of the autoionizing state is given by the square of the autocorrelation function [11]

$$P(t)=|\langle\Psi_i(r_1,r_2)|\Psi(r_1,r_2;t)\rangle_{r_1,r_2}|^2. \tag{18}$$

In Fig. 2 we compare the time evolution $P(t)$ calculated via Eq. (18) with the exponential behavior, $P(t)\sim\exp(-\Gamma t)$, corresponding to the decay width $\Gamma=1.167\times10^{-3}$ a.u. as derived via the golden rule in [14]. Fitting an exponential to the time-dependent population $P(t)$ yields the width $\Gamma=1.123\times10^{-3}$ a.u., which agrees to within less than 4% with the value of Ref. [14].

For an electron colliding with a hydrogen atom ($Z=1$), the target electron is initially described by the radial wave function $\varphi_1(r)$ of the $1s$ hydrogen bound state,

$$\varphi_1(r)=2r\ e^{-r}, \tag{19}$$

and the projectile electron is represented by a Gaussian wave packet centered at a position s sufficiently far from the target electron,

$$\Psi(r_1,r_2;t=0)=\frac{1}{(2\pi b^2)^{1/4}}\exp[-ik_0r_1]\times\exp\left[-\frac{(r_1-s)^2}{4b^2}\right]\varphi_1(r_2). \tag{20}$$

The wave packet has an average momentum k_0 of the projectile electron and a spread b in coordinate space, corresponding to a spread $\Delta k=1/(2b)$ in the momentum and a k_0-dependent spread in energy,

$$\Delta E=k_0\Delta k=\frac{k_0}{2b}. \tag{21}$$

The typical behavior of the time-iterated wave function is shown in Fig. 3 for an incident wave packet with average momentum $k_0=2$ a.u. centered at $s=10$ a.u. with a width $b=2.5$ a.u. in coordinate space. The iteration was performed with a time step $\Delta t=0.05$. Figures 3(a) and 3(b) show the two-electron densities $|\Psi(r_1,r_2;t)|^2$ at different times for the symmetrized (singlet) and antisymmetrized (triplet) case, respectively. The density reaches its maximum of compression in coordinate space at a time of about $t=5$. At $t=15$, different zones of the two-electron density can be distinguished: Most of the density is contained in outgoing wave packets along the coordinate axes, but, for $S=0$, a certain fraction is concentrated in a broad wave packet around $r_1=r_2$ which travels along rays emanating from the origin. A similar behavior of the wave function at large times was observed by Bottcher [23] in a time-dependent calculation for the collinear model. Bottcher assigned the wave packets along the axes to elastic and inelastic scattering and interpreted the broad packet along $r_1=r_2$ as the result of double escape. A direct evaluation of the probability for double escape from such a wave function in coordinate space is, however, problematic, because components from highly excited Rydberg states of the target extend to large distances in coordinate space. In the present paper we calculate the component of the wave function corresponding to double escape by projecting out the bound-bound and bound-continuum parts—see Sec. IV.

It is interesting to study the time evolution of electron-electron correlations. These can conveniently be described with the help of the reduced density operator

$$\tilde\rho(r_2,r_2',;t)\equiv\int dr_1\Psi^*(r_1,r_2';t)\Psi(r_1,r_2;t), \tag{22}$$

which contains all the information about the subsystem consisting of one of the electrons (here the electron with coordinate r_2). For a simple uncorrelated product wave function $\Psi=\psi_1(r_1)\psi_2(r_2)$, the integration over r_1 in (22) yields unity (for normalized ψ_1) and $\tilde\rho$ is simply the density matrix for the pure state described by the one-electron wave function $\psi_2(r_2)$, and it obeys $[\tilde\rho]^2=\tilde\rho$. Any deviation from a simple uncorrelated product leads to a violation of this equation, because $\tilde\rho$ then describes a mixed state. The relevant information is contained in the difference $K(r_2,r_2';t)$ of the reduced density operator and its square,

$$K(r_2,r_2';t)\equiv\tilde\rho(r_2,r_2';t)-\int\tilde\rho(r_2,r_2'';t)\tilde\rho(r_2'',r_2';t)dr_2'', \tag{23}$$

and the trace of $K(r_2,r_2';t)$ defines a convenient quantitative measure of correlation

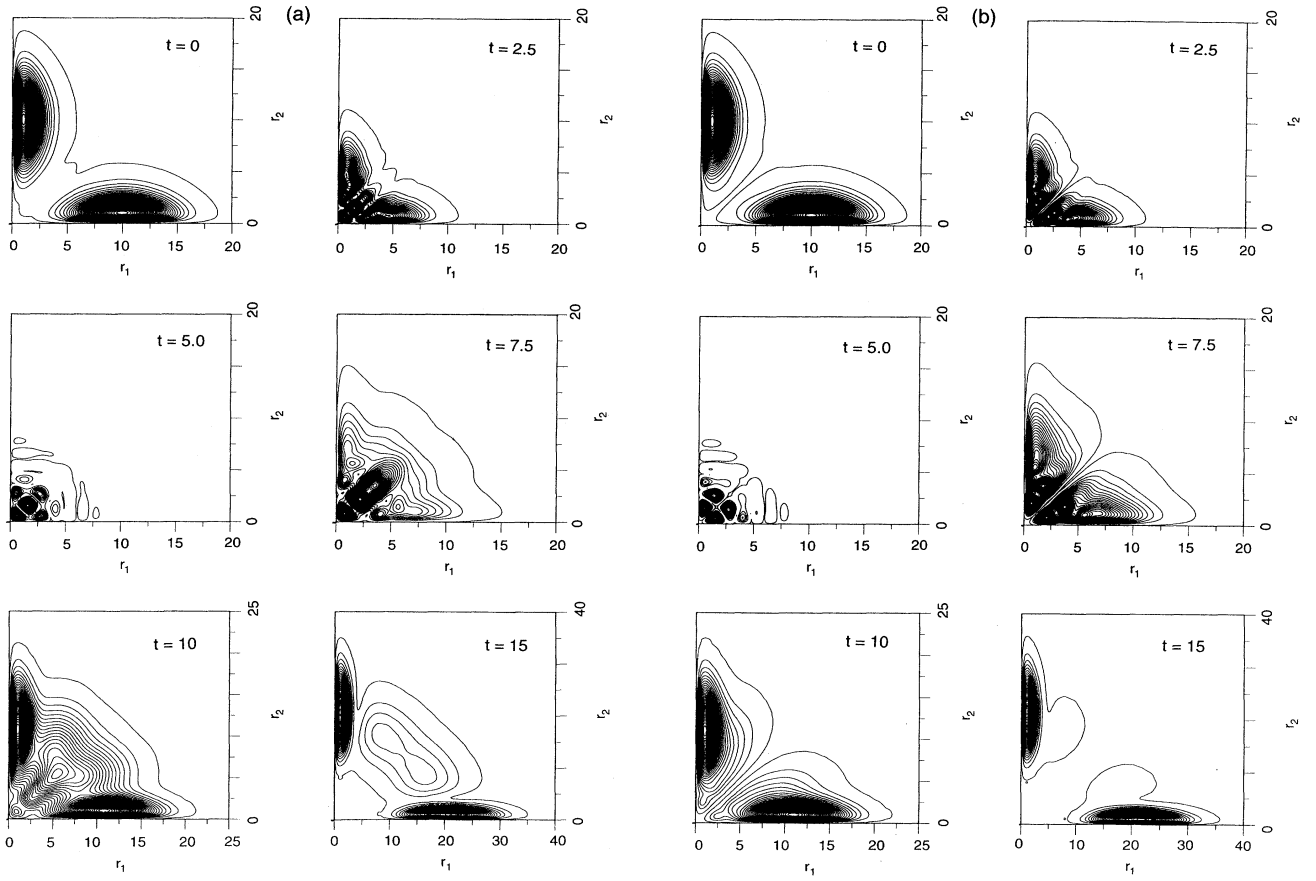

FIG. 3. (a) Time evolution of the density $|\Psi(r_1,r_2;t)|^2$ for an initial state (20) describing an incoming electron with average momentum $k_0=2$ in a Gaussian wave packet of width $b=2.5$ in coordinate space approaching a hydrogen atom ($Z=1$) in its ground state (singlet case). (b) Same as (a) but for the triplet case.

$$\mathscr{E}(t)\equiv\int dr_2 K(r_2,r_2;t)=1-\int dr_2 dr_2''|\tilde{\rho}(r_2,r_2'';t)|^2. \tag{24}$$

$\mathscr{E}(t)$ is zero for a completely uncorrelated (pure) state of the two-electron system and can assume a maximal value of unity. The correlation measure $\mathscr{E}$ does not depend on the representation used to express the two-electron wave function. Symmetrization (5) or antisymmetrization (6) of an uncorrelated product wave function, in order to satisfy the requirements of the Pauli principle, yields a value $\frac{1}{2}$ for $\mathscr{E}(t)$. Thus any departure of $\mathscr{E}(t)$ from $\frac{1}{2}$ for a properly symmetrized or antisymmetrized two-particle wave function indicates correlations beyond the fundamental requirements of the Pauli principle.

Figure 4 shows the evolution of the correlation measure $\mathscr{E}(t)$ for incident wave packets (20) with a width $b=2.5$ starting at $s=15$ for various average momenta k_0 of the incident electron. The iteration was performed with time steps given by $\Delta t=0.1/k_0$. The abscissa in Fig. 4 shows the scaled time $k_0 t$, so a free particle starting with the center of the wave packet reaches the origin at $k_0 t=15$. The correlation of the wave function increases during the reaction and saturates at a constant value. A similar behavior of correlations has recently been observed by Grobe, Rzążewski, and Eberly [27] in the regularized collinear model. In Fig. 4 we see that correlation effects are much stronger in the singlet states than in the triplet states, where the effect of the electron-electron interaction is suppressed, because the wave function vanishes on the diagonal $r_1=r_2$. Comparing the three values of k_0 shows that the correlation measure in the

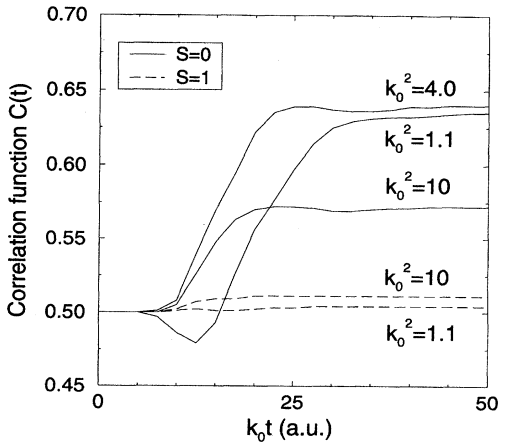

FIG. 4. Time dependence of the correlation measure (24) for various asymptotic average momenta k_0 of the incoming electron.

singlet states rises to quite a high value near threshold and at $k_0^2=4$, whereas the increase is slower and to a smaller value at the higher energy, $k_0^2=10$. Note that $k_0^2=4$ is near the maximum of the probability for double escape, see Sec. IV C.

IV. SCATTERING AND IONIZATION PROBABILITIES

As the normalized wave function $\Psi(r_1,r_2;t)$ evolves from (20), the time-dependent probability $p_n(t)$ for finding one electron in the hydrogenic bound state φ_n and the other electron in a continuum state is given by

$$p_n(t)=2\left\{\int dr_1|\langle\Psi(r_1,r_2;t)|\varphi_n(r_2)\rangle_{r_2}|^2 - \sum_{n'=1}^{\infty}|\langle\Psi(r_1,r_2;t)|\varphi_n(r_2)\varphi_{n'}(r_1)\rangle_{r_1,r_2}|^2\right\}. \tag{25}$$

The subscripts on the scalar products refer to the coordinate over which integration is performed. The first term in the curly brackets in Eq. (25) gives the probability of finding electron 2 in the bound state φ_n while electron 1 can be in any bound or continuum state. The second term must therefore be subtracted to project out the probability that both electrons are in a bound state. For large times there is only a small probability of both electrons being in a bound state, because this implies a total energy below ionization threshold and hence can only come from the low-energy tail of the initial wave packet. There can, however, be a substantial transient contribution from such doubly bound states, and its subtraction greatly improves convergence [25]. The probability for finding electron 1 in the bound state φ_n and electron 2 in the continuum is given by the expression in the curly brackets with the coordinates r_1 and r_2 exchanged. This gives the same value of the curly brackets, provided the total wave function $\Psi(r_1,r_2;t)$ is properly symmetrized according to (5) or antisymmetrized according to (6); hence the indistinguishability of the two electrons is correctly accounted for by the factor 2 on the right-hand side of (25). The time-dependent probability $p_{(e,2e)}(t)$ for finding both electrons in a continuum state is obtained by subtracting from unity all the probabilities $p_n(t)$ of (25) for finding one and only one electron in a bound state φ_n, as well as the probability for finding both electrons in bound states,

$$p_{(e,2e)}(t)=1-\sum_{n=1}^{\infty}p_n(t) - \sum_{n,n'=1}^{\infty}|\langle\Psi(r_1,r_2;t)|\varphi_n(r_2)\varphi_{n'}(r_1)\rangle_{r_1,r_2}|^2. \tag{26}$$

The time-independent probabilities,

$$\mathscr{P}_n=\lim_{t\to\infty}p_n(t), \quad \mathscr{P}_{(e,2e)}=\lim_{t\to\infty}p_{(e,2e)}(t), \tag{27}$$

are obtained from the time-dependent probabilities (25) and (26) by following the evolution until convergence is achieved. Unless otherwise stated, calculations were performed for an initial wave packet (20) of width $b=8$ a.u. in coordinate space and starting at a distance $s=45$ a.u. The probabilities obtained in this way are functions of the initial average energy or momentum k_0 of the projectile electron. The probabilities for elastic scattering, inelastic scattering to the $n=2$ and 3 channels, and for ionization are listed in Table I for values of k_0^2 ranging from 1 to 17.5. The probabilities listed in Table I are related to the bare probabilities appearing in Eqs. (7), (8) by convolution with a Gaussian of width $1/(2b)$ ($\equiv 0.0625$ a.u.) in momentum, corresponding to the uncertainty of the initial wave packet. The bare probabilities defined with respect to fixed incoming energy or momentum can be derived from the probabilities (27) by deconvolution. Except for the ionization probability near threshold, this was found to be unnecessary, because the bare probabilities are smooth functions and the uncertainty width of the wave packet was always much smaller than the range over which they vary substantially. The special case of ionization probabilities near threshold is treated in Sec. IV D.

A. Elastic scattering

In order to compare the scattering and reaction probabilities of the present calculation with the results of previous calculations based on the three-dimensional picture [20,22], we transform the cross sections given by these authors to dimensionless probabilities. For inelastic scattering and ionization, this merely means dividing the cross sections by the area π/k^2, but for the elastic channel, the dimensionless probability (7) is related to the cross sections (10) by

$$P_1=1-\frac{k^2}{\pi}(\sigma_{\rm tot}-\sigma_1), \tag{28}$$

where $\sigma_{\rm tot}=\Sigma_{n=1}^{\infty}\sigma_n+\sigma_{(e,2e)}$ is the total cross section appearing in (11).

The resulting probabilities for singlet symmetry are shown in Fig. 5 as a function of $k^2=2E_{\rm in}$, where $E_{\rm in}$ is the impact energy of the incoming electron. Near $k^2=1$, the elastic scattering probability P_1 is in excellent agreement with the results of Bhatia, Schneider, and Temkin [22], obtained by a T-matrix variational principle, and those of Callaway and Oza [20], who solved the stationary Schrödinger equation by expansion methods numerically on a grid. Our probabilities show a smoother dependence on the energy of the incident electron whereas the probabilities calculated by these authors show oscillations, which cannot be attributed to physical grounds.

B. Inelastic scattering

For total energies sufficiently high above the breakup threshold $E=0$ (corresponding to $E_{\rm in}=\frac{1}{2}k^2=\frac{1}{2}$ for the incoming electron), the probability for exciting the target from the ground state to an excited state $n>1$ may be expected to be proportional to $1/n^3$ as is typical in a Rydberg series. This is indeed the case as is illustrated in Fig. 6, where the open diamonds show the inelastic scattering probabilities P_n for $n=2,\ldots,7$ at $k^2=4$ plotted against n in a doubly logarith-

TABLE I. Probabilities for elastic and inelastic scattering and for ionization (27). k_0^2 is the square of the average asymptotic momentum of the projectile electron in a wave packet with a momentum spread $\Delta k = \frac{1}{16}$ a.u. [cf. (21)].

	Singlet ($S=0$)				Triplet ($S=1$)			
k_0^2	$\mathcal{P}_1$	$\mathcal{P}_2$	$\mathcal{P}_3$	$\mathcal{P}_{(e,2e)}$	$\mathcal{P}_1$	$\mathcal{P}_2$	$\mathcal{P}_3$	$\mathcal{P}_{(e,2e)}$
1.0	0.797	0.149	0.0222	0.0065	0.997	0.003	0.0001	0.0000
1.1	0.762	0.161	0.0314	0.0175	0.995	0.005	0.0003	0.0001
1.2	0.733	0.163	0.0368	0.0341	0.993	0.006	0.0005	0.0001
1.3	0.709	0.161	0.0393	0.0541	0.991	0.008	0.0008	0.0002
1.5	0.673	0.153	0.0395	0.0958	0.987	0.010	0.0013	0.0007
1.75	0.643	0.140	0.0376	0.141	0.982	0.013	0.0020	0.0017
2.0	0.630	0.127	0.0343	0.174	0.977	0.016	0.0026	0.0032
2.25	0.622	0.116	0.0313	0.199	0.972	0.017	0.0031	0.0050
2.5	0.625	0.105	0.0283	0.213	0.968	0.018	0.0035	0.0069
2.75	0.628	0.097	0.0259	0.223	0.964	0.020	0.0038	0.0090
3.0	0.635	0.089	0.0237	0.228	0.961	0.020	0.0040	0.0109
3.25	0.646	0.082	0.0216	0.229	0.959	0.021	0.0041	0.0127
3.5	0.653	0.076	0.0204	0.230	0.956	0.021	0.0045	0.0147
3.75	0.664	0.071	0.0189	0.227	0.954	0.021	0.0045	0.0163
4.0	0.675	0.066	0.0177	0.223	0.953	0.021	0.0046	0.0178
4.5	0.695	0.058	0.0155	0.216	0.951	0.020	0.0046	0.0205
5.0	0.714	0.053	0.0136	0.206	0.949	0.020	0.0044	0.0226
5.5	0.732	0.048	0.0122	0.195	0.948	0.020	0.0044	0.0239
6.0	0.748	0.043	0.0114	0.187	0.947	0.018	0.0044	0.0256
7.0	0.773	0.039	0.0097	0.169	0.946	0.019	0.0042	0.0275
8.0	0.800	0.033	0.0083	0.151	0.948	0.017	0.0039	0.0282
9.0	0.820	0.029	0.0073	0.137	0.949	0.016	0.0037	0.0282
10.0	0.835	0.026	0.0066	0.126	0.950	0.015	0.0034	0.0288
12.5	0.869	0.020	0.0050	0.101	0.954	0.012	0.0029	0.0279
15.0	0.888	0.018	0.0044	0.0855	0.956	0.012	0.0028	0.0270
17.5	0.908	0.014	0.0034	0.0707	0.961	0.010	0.0022	0.0247

mic plot. The straight line through the open diamonds demonstrates proportionality to $1/n^3$. Closer to threshold, however, the Rydberg-type behavior of the inelastic scattering probabilities breaks down, because a high excitation of the bound electron is accompanied by a deexcitation of the projectile electron to energies close to the continuum limit, and effects of two-electron correlation are important. This is illustrated by the solid dots representing the inelastic scattering probabilities at threshold. They are closer to being proportional to $1/n^{3.5}$ for high n. For energies sufficiently above the breakup threshold, the inelastic scattering probabilities

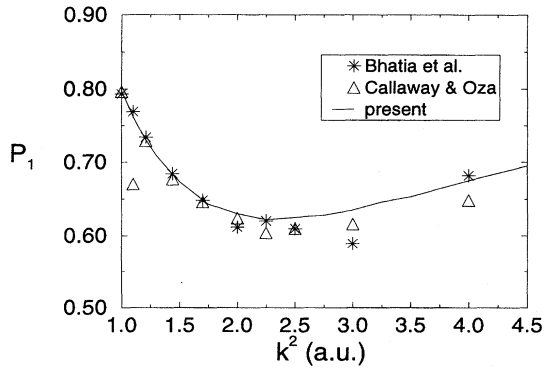

FIG. 5. Probability P_1 ($S=0$) for elastic scattering of an electron by hydrogen in the s-wave model as a function of $k^2=2E_{\rm in}$, where k is the asymptotic momentum and $E_{\rm in}$ is the impact energy of the projectile electron. The asterisks and triangles are derived from the cross sections given by Bhatia, Schneider, and Temkin [22] and by Callaway and Oza [20] via Eq. (28).

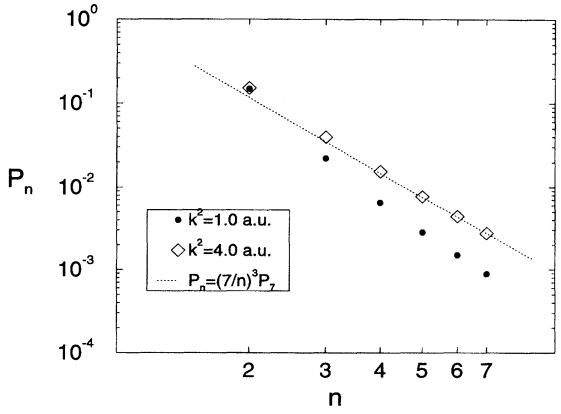

FIG. 6. Doubly logarithmic plot of the inelastic scattering probabilities P_n ($S=0$) for impact energies above ($k^2=4$) and at ($k^2=1$) the breakup threshold.

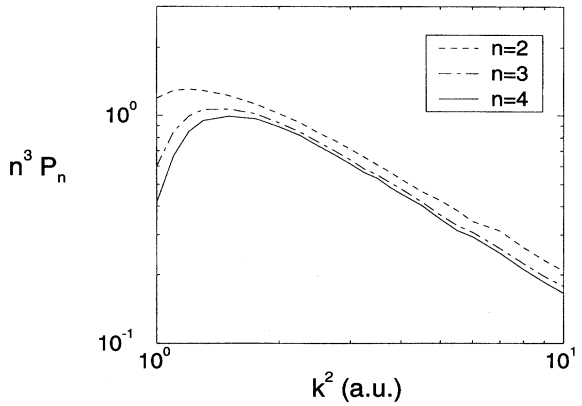

FIG. 7. Doubly logarithmic plot of the inelastic scattering probabilities P_n $(S=0)$, normalized by n^3, as a function of $k^2=2E_{\rm in}$.

are inversely proportional to the impact energy of the projectile electron, as illustrated in Fig. 7. Note that the Born approximation and Bethe's theory predict the high-energy behavior of inelastic cross sections in realistic situations to be proportional to $(\ln E_{\rm in})/E_{\rm in}$ [28]; this is closer to the behavior of the dimensionless probabilities in the one-dimensional s-wave model than to the behavior of the cross sections of its three-dimensional interpretation, which are proportional to $1/E_{\rm in}^2$ due to the additional factor describing the decreasing weight of the component with vanishing total angular momentum towards higher energies.

A comparison of the present results for excitation to the $n=2$ and 3 states with the corresponding probabilities derived from [20] is shown in Fig. 8. Agreement is good except for P_2 just above threshold, where the results of [20] lie a little above our values.

C. Ionization

One difficulty in using Eq. (26) to extract the time-dependent probability $p_{(e,2e)}(t)$ and eventually the time-independent ionization probability is performing the infinite sum over $p_n(t)$. Because of the finite evolution time of the two-electron wave function and the finite size of the box in

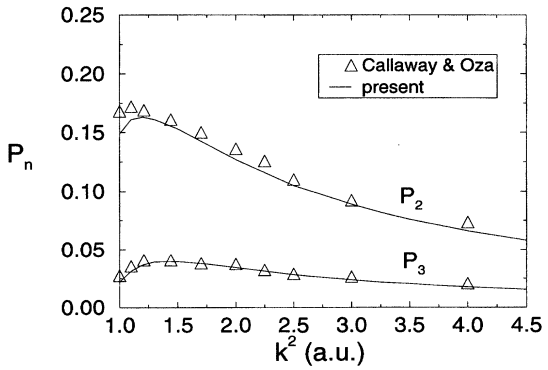

FIG. 8. Comparison of the inelastic scattering probabilities P_2, P_3 $(S=0)$ obtained in the present calculation with the results derived from the corresponding cross sections of Callaway and Oza [20] via Eqs. (10) and (7).

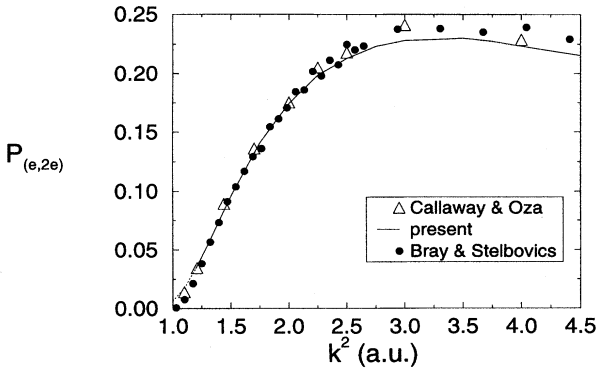

FIG. 9. Probability $\mathscr{P}_{(e,2e)}$ for electron-impact ionization of hydrogen for singlet symmetry in the s-wave model (solid line). The triangles and solid dots were obtained from the corresponding cross sections given by Callaway and Oza [20] and by Bray and Stelbovics [30] according to (13).

coordinate space, projection onto bound target states is possible only for a finite number $n\leq n_0$. We chose $n_0=7$ and estimated the residual sum $\Sigma_{n=8}^{\infty}p_n(t)$ by extrapolating the behavior of the $p_n(t)$ using a power law. The power involved was not rigidly chosen to be -3, but adapted to the observed behavior of the probabilities $p_n(t)$, $n\leq 7$ in accordance with the discussion of Fig. 6. We found that following the evolution of the time-dependent probability $p_{(e,2e)}(t)$ until it converged in time yielded more stable and reliable results than simply deducing the ionization probability from the scattering probabilities via the conservation law (8) or the optical theorem (11), as done by Callaway and Oza [20]. This method has also been applied by Isele in order to derive ionization cross sections at a few impact energies in the collinear and in the s-wave model [29].

The ionization probabilities derived for the singlet case are shown in Fig. 9 for values of k^2 ranging from threshold $(k^2=1)$ to $k^2=4.5$ a.u. and compared with the results of Callaway and Oza [20] and Bray and Stelbovics [30]. In both [20] and [30] the ionization cross sections were derived indirectly from the elastic and inelastic cross sections via the optical theorem (11). The present calculation reproduces the behavior of these results quite well for $k^2<2.5$, and it is free from the unphysical oscillations, which Bray and Stelbovics attribute to spurious resonances connected with the pseudostates they use to approximate the one-electron continuum. For $k^2>3$ our results are systematically slightly below those of Ref. [30] by about 0.015. This may indicate that the sum over all inelastic excitations is slightly underestimated in [30]. The ionization probability goes through a broad maximum between $k^2=3$ and 4. The two-electron correlations as illustrated in Fig. 4 are more pronounced here than at higher energies.

Figure 10 shows the singlet, triplet, and spin-averaged probabilities,

$$\frac{\sigma_0}{4}[P_{(e,2e)}^{(S=0)}+3P_{(e,2e)}^{(S=1)}], \tag{29}$$

of the present one-dimensional s-wave model in comparison with the experimental data of Shah, Elliott, and Gilbody [17]

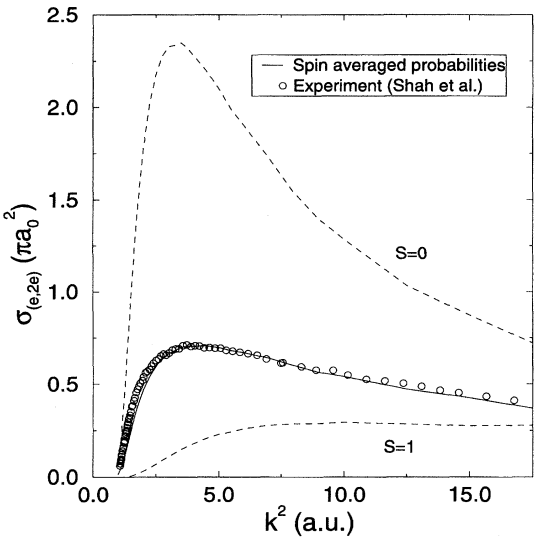

FIG. 10. Singlet, triplet, and spin-averaged probabilities for electron-impact ionization in the s-wave model, multiplied by the energy-independent area $\sigma_0 = 10.1\pi$ a.u. [cf. (29)]. The empty circles show the experimental integrated ionization cross sections of Shah, Elliott, and Gilbody [17].

for the electron-impact ionization of real hydrogen atoms. These data are still generally accepted as accurate, although Shyn [31] has recently presented ionization cross sections differing somewhat from the results of Ref. [17]. The dimensionless probabilities of the s-wave model are multiplied by one energy-independent area $\sigma_0 = 10.1\pi$ a.u., so that the height of the maximum is fitted to the experimental value. Except for the region just above threshold, which we discuss in the next subsection, the spin-averaged probabilities reproduce the experimental energy dependence remarkably well. This is perhaps surprising, considering that numerous attempts to reproduce the ionization cross section for energies near and above the maximum at $k^2 \approx 4$ have been unsuccessful over the years. The present calculation gives a better account of the shape of the experimental ionization cross section near and above the maximum than all approximations previously studied, and it is only surpassed by the recent convergent close coupling calculation of Bray and Stelbovics [4], which in principle involves no approximation and represents a true breakthrough in the description of ionization processes. The success of the present model calculation indicates that the net effects of angular correlations in the integrated ionization cross sections for real hydrogen are small at energies near and above the maximum. Note that the ionization cross sections (13) derived with the potential (4) in the three-dimensional picture do not give a good account of the observed energy dependence, because the additional factor π/k^2 describing the decreasing weight of the component with vanishing total angular momentum leads to a too rapid falloff towards higher energies.

D. Threshold behavior

The threshold behavior of ionization cross sections has been a subject of great interest since Wannier's famous paper [32]. It is generally accepted that the cross section for electron-impact ionization of hydrogen behaves as $E^{1.127}$, and this can be understood on the basis of the classical motion of the electrons escaping in opposite directions from the nucleus [32,15]. The s-wave model is not well suited to describe this situation, where angular correlations are very important. It is nevertheless of considerable interest to study the threshold behavior in the s-wave model, because in the classical version of this model ionization is dynamically forbidden for a finite range of energies above threshold [12]. For two spherical electrons moving classically away from the nucleus with small positive individual energies, the inner electron must be faster than the outer electron which is overtaken and falls back into bound motion. The dynamical threshold for the electron-impact ionization of hydrogen in the classical description lies above the energetic threshold by one-third of the initial binding energy of the target electron. When the target electron is initially in the ground state, the energetic threshold is $E_{\rm in} = \frac{1}{2}$ $(k^2 = 1)$ and the dynamic threshold for classical ionization is $E_{\rm in} = \frac{2}{3}$ $(k^2 = \frac{4}{3})$ [12].

In the present time-dependent method, the wave function $\Psi(r_1, r_2; t)$ has a spread in energy and momentum, which is determined by the width of the initial wave packet (20). The momentum distribution as given by the absolute square of the initial wave packet in momentum space is a Gaussian with the profile function

$$w(k-k_0) = b\sqrt{2/\pi}\,\exp[-2b^2(k-k_0)^2]. \tag{30}$$

The calculation does not yield the bare ionization probability $P_{(e,2e)}(k)$ but a convoluted probability

$$\mathscr{P}_{(e,2e)}(k_0) = \int_1^\infty P_{(e,2e)}(k) w(k-k_0)\,dk. \tag{31}$$

The lower limit of the integral over the asymptotic momentum k of the projectile electron is the threshold value $k = 1$, because $P_{(e,2e)}(k)$ vanishes for smaller k.

For the present calculations based on a width $b = 8$ a.u. in coordinate space, the width of the profile function (30) in momentum space is 0.0625 which is sufficiently small to be neglected over most of the energy range, but not of course at threshold. The bare ionization probability vanishes at threshold and may be approximated by a monomial,

$$P_{(e,2e)}(k) = \begin{cases} C(k-1)^\alpha, & k \geq 1 \\ 0, & k < 1 \end{cases} \tag{32}$$

with a constant factor C. The threshold behavior of the ionization probability as function of the total energy $E = (k^2-1)/2 \approx k-1$ is given by the same power law. Inserting the power law (32) into (31) shows that we obtain a convoluted ionization probability $\mathscr{P}_{(e,2e)}(k_0)$ which is proportional to $(k_0-1)^\alpha$, if we choose the width parameter b inversely proportional to $k_0 - 1$. For $b(k_0) = b_0/(k_0-1)$ we have

$$\mathscr{P}_{(e,2e)}(k_0) = C\, J(\alpha; b_0)(k_0-1)^\alpha, \tag{33}$$

where $J(\alpha; b_0)$ is a constant given by

$$J(\alpha; b_0) = \sqrt{2b_0^2/\pi}\int_0^\infty \tau^\alpha \exp[-2b_0^2(\tau-1)^2]\,d\tau. \tag{34}$$

TABLE II. Convoluted ionization probabilities (31). The width b of the initial wave packet describing the projectile electron in coordinate space varies as $b=0.5/(k_0-1)$ with its average asymptotic momentum k_0. The rightmost column shows the results obtained when the electron-electron interaction potential $1/r_>$ of the s-wave model is replaced by the short-ranged interaction potential $\exp(-0.2r_>)/r_>$.

	$\mathscr{P}_{(e,2e)}$	
k_0-1	s-wave potential	Short-ranged potential
$\frac{1}{16}$	0.0217	0.0346
$\frac{1}{15}$	0.0238	0.0371
$\frac{1}{14}$	0.0262	0.0399
$\frac{1}{13}$	0.0291	0.0431
$\frac{1}{12}$	0.0324	0.0467
$\frac{1}{11}$	0.0364	0.0509

The convoluted ionization probabilities (31) calculated with the width parameter $b_0=0.5$ in the range $b=8.0$ ($k_0-1=\frac{1}{16}$) to $b=5.5$ ($k_0-1=\frac{1}{11}$) are listed in Table II and shown as solid dots in the doubly logarithmic plot in Fig. 11. Only singlet states are important here, because the ratio of the triplet to singlet ionization probabilities vanishes towards threshold (see Table I).

The behavior of the solid dots in Fig. 11 is best fitted by $\mathscr{P}_{(e,2e)}=1.05E^{1.4}$, corresponding to a threshold behavior $P_{(e,2e)}=0.79E^{1.4}$ of the bare ionization probabilities according to Eqs. (33) and (32), which is somewhat suppressed compared to the Wannier results $P_{(e,2e)}\propto E^{1.127}$. This is understandable, because the motion along the diagonal $r_1=r_2$ is infinitely unstable, and near threshold ionization is dynamically forbidden in the classical version of the s-wave model. Figure 12 illustrates the threshold behavior of the deconvoluted ionization probability $P_{(e,2e)}$ (dashed line) which merges into the convoluted probability $\mathscr{P}_{(e,2e)}$ near $k^2=1.4$. Due to the narrow width of the incoming wave packet in energy, deconvolution is not necessary at higher energies. We have checked the reliability of this method of extracting an exponent for the threshold behavior of the ionization probability by repeating the calculation for a fictitious model of two particles interacting with the nucleus via a $1/r$ potential, but with each other via the short-ranged potential $\exp(-0.2r_>)/r_>$ replacing the interaction term $1/r_>$ in (4). The asymptotic solution of the time-independent Schrödinger equation for two escaping electrons is known to be a product of two Coulomb functions in this case, and the probability for ionization is proportional to the total energy E near threshold [33]. The corresponding convoluted ionization probabilities are listed in the right-hand column of Table II and shown as empty diamonds in Fig. 11. Their behavior is well fitted by an exponent $\alpha=1$, as expected.

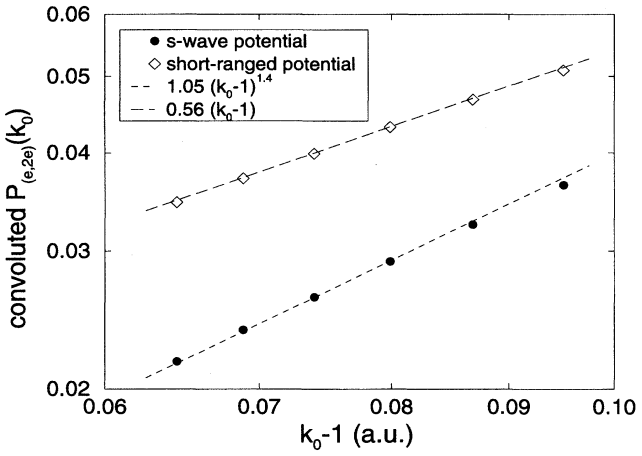

FIG. 11. Doubly logarithmic plot of the convoluted ($S=0$) ionization probabilities $\mathscr{P}(k_0)$ defined by (31), (30) with wave packet widths b (in coordinate space) inversely proportional to the average asymptotic momentum (relative to threshold) k_0-1 of the projectile electron, $b=0.5/(k_0-1)$. The solid dots are the results for the s-wave model. The empty diamonds are the corresponding results obtained when the long-ranged electron-electron interaction potential $1/r_>$ of the s-wave model is replaced by the short-ranged potential $\exp(-0.2r_>)/r_>$. The short dashed line shows proportionality to $(k_0-1)^{1.4}$, while the long dashed line shows the linear dependence on (k_0-1) which is expected for the short-ranged interaction potential.

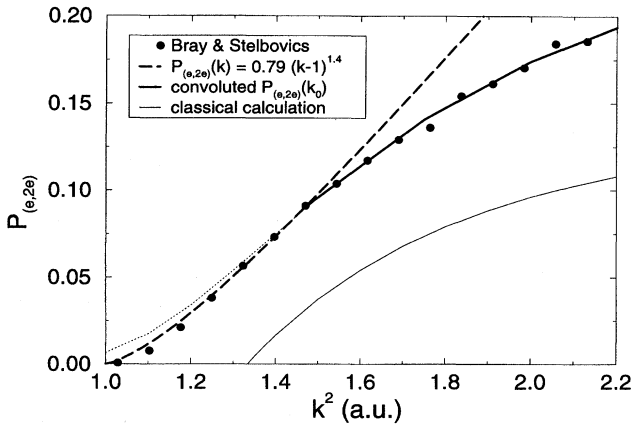

FIG. 12. Deconvoluted ($S=0$) ionization probability $P_{(e,2e)}=0.79E^{1.4}$ (dashed), which merges into the convoluted probabilities $\mathscr{P}_{(e,2e)}$ of Table I near $k^2=1.4$. The dotted line shows the continuation of the convoluted probabilities towards lower energies. The dots are the probabilities derived from the cross sections of Bray and Stelbovics [30] according to (13). The thin solid line shows the classical ionization probabilities obtained in [12].

V. CONCLUSION

We have integrated the time-dependent Schrödinger equation for continuum states in the s-wave model of two-electron atoms. The method allows us to study the evolution of two-particle correlations in the wave function and yields probabilities for elastic and inelastic scattering as well as for electron-impact ionization. It produces stable and reliable results and compares favorably with the methods based on the time-independent Schrödinger equation. An important advantage of the time-dependent technique for studying ionization is that it does not require knowledge of the asymptotic wave functions for two electrons in the continuum, which are known only in various limits and approximations.

For total energies E close to the breakup threshold $E=0$, the probability for electron-impact ionization of hydrogen is roughly proportional to $E^{1.4}$ in the s-wave model.

This is somewhat suppressed in comparison with the Wannier law $E^{1.127}$ for real hydrogen. Note that in the classical version of the s-wave model, electron-impact ionization of hydrogen from its ground state is dynamically forbidden for $E<1/6$ a.u.

The spin-averaged probabilities for electron-impact ionization of hydrogen in the s-wave model reproduce the shape of the experimentally observed ionization cross sections remarkably well for energies near and above the maximum. This agreement is in fact better than has so far been achieved in approximate descriptions of the ionization process, and it is only surpassed by the in principle exact *ab initio* calculation of Bray and Stelbovics [4].

The s-wave model is perhaps the simplest model of two electrons interacting with a nucleus and with each other via long-ranged Coulomb forces; it is well suited for studying qualitative aspects of the physics of real two-electron atoms, and as a testing ground for calculational techniques. Having established in Ref. [14] that this model gives a very good quantitative description of the $1sns$ bound states of real helium, we now observe a realistic behavior of the probabilities for ionizing hydrogen. For energies not too close to the ionization threshold, where angular correlations are definitely important, the s-wave model does appear to contain some realistic physics.

ACKNOWLEDGMENTS

We thank the Deutsche Forschungsgemeinschaft (Az: Fr 591/3-3) for financial support and A. Isele for making available her Diploma thesis [29]. W. I. especially thanks the Studienstiftung des deutschen Volkes for support and encouragement.

[1] M. Domke *et al.*, Phys. Rev. Lett. **66**, 1306 (1991).
[2] M. Domke, G. Remmers, and G. Kaindl, Phys. Rev. Lett. **69**, 1171 (1992).
[3] M. Domke, K. Schulz, G. Remmers, A. Gutiérrez, G. Kaindl, and D. Wintgen, Phys. Rev. A **51**, R4309 (1995).
[4] I. Bray and A. T. Stelbovics, Phys. Rev. Lett. **70**, 746 (1993).
[5] Y. Gu and J.-M. Yuan, Phys. Rev. A **47**, R2442 (1993).
[6] M. Brauner, J. S. Briggs, and H. Klar, J. Phys. B **22**, 2265 (1989).
[7] K. Richter and D. Wintgen, Phys. Rev. Lett. **65**, 1965 (1990); J. Phys. B **24**, L565 (1991).
[8] D. Wintgen, K. Richter, and G. Tanner, Chaos **2**, 19 (1992).
[9] G. Handke, M. Draeger, and H. Friedrich, Physica A **197**, 113 (1993).
[10] R. Grobe and J. H. Eberly, Phys. Rev. A **48**, 4664 (1993).
[11] S. L. Haan, R. Grobe, and J. H. Eberly, Phys. Rev. A **50**, 378 (1994).
[12] G. Handke, M. Draeger, W. Ihra, and H. Friedrich, Phys. Rev. A **48**, 3699 (1993).
[13] G. Handke, Phys. Rev. A **50**, R3561 (1994).
[14] M. Draeger, G. Handke, W. Ihra, and H. Friedrich, Phys. Rev. A **50**, 3793 (1994).
[15] J.-M. Rost, Phys. Rev. Lett. **72**, 1998 (1994).
[16] J.-M. Rost, J. Phys. B **27**, 5923 (1994).
[17] M. B. Shah, D. S. Elliott, and H. B. Gilbody, J. Phys. B **20**, 3501 (1987).
[18] A. Temkin, Phys. Rev. **126**, 130 (1962).
[19] R. Poet, J. Phys. B **11**, 3081 (1978); **13**, 2995 (1980); **14**, 91 (1981).
[20] J. Callaway and D. H. Oza, Phys. Rev. A **29**, 2416 (1984).
[21] I. Bray and A. T. Stelbovics, Phys. Rev. Lett. **69**, 53 (1992).
[22] A. K. Bhatia, B. I. Schneider, and A. Temkin, Phys. Rev. Lett. **70**, 1936 (1993).
[23] C. Bottcher, J. Phys. B **14**, L349 (1981).
[24] C. Bottcher, Adv. At. Mod. Phys. **20**, 241 (1985).
[25] W. Ihra, doctoral thesis, Technical University Munich, Verlag Shaker, Aachem, 1995.
[26] W. H. Press, B. P. Flannery, S. A. Teukolsky, and W. T. Vetterling, *Numerical Recipes* (Cambridge University Press, Cambridge, England, 1986).
[27] R. Grobe, K. Rzążewski, and J. H. Eberly, J. Phys. B **27**, L503 (1994).
[28] M. Inokuti, Rev. Mod. Phys. **43**, 297 (1971).
[29] A. Isele, Diploma thesis, Albert-Ludwigs-Universität, Freiburg im Breisgau, 1994 (unpublished).
[30] I. Bray and A. T. Stelbovics, At. Data Nucl. Data Tables **58**, 67 (1994).
[31] T. W. Shyn, Phys. Rev. A **45**, 2951 (1992).
[32] G. H. Wannier, Phys. Rev. **90**, 817 (1953).
[33] A. R. P. Rau, Phys. Rev. A **4**, 207 (1971).